

Field-Oriented Control of a Three-Phase Wireless Power Transfer System Transmitter

Mehanathan Pathmanathan¹, Member, IEEE, Shuang Nie¹, Student Member, IEEE,
Netan Yakop¹, and Peter W. Lehn, Senior Member, IEEE

Abstract—This paper presents a method of designing a three-phase wireless power transfer (WPT) transmitter analogous to the stator windings of a three-phase, two-pole electrical machine. A method of deriving the required transmitter coil currents based on lateral receiver misalignment is presented, wherein the transmitter currents are decomposed into direct and quadrature axis components. This decomposition simplifies the derivation of the transmitter currents required to minimize copper losses for a wide range of receiver misalignment by reorienting the transmitter magnetic field toward the receiver. Based on the required transmitter current, the required series compensation capacitors and transmitter voltage sources needed for unity power factor operation are calculated. Simulation results are shown for a 3.3-kW system utilizing a receiver-side voltage-doubling rectifier and 300-V battery. Finally, experimental results on a 1-kW prototype are shown, where a coil efficiency of 95.17% at perfect receiver alignment and 90.52% at 20-cm lateral misalignment was measured.

Index Terms—Contactless power transfer, field-oriented control, magnetically coupled system.

I. INTRODUCTION

ELECTRIC vehicles (EVs) present an attractive alternative to their internal combustion engine based counterparts as they alleviate the emissions of greenhouse gases to the environment. The greatest barrier to the widespread adoption of EVs is range anxiety, which is mostly due to the lack of easily accessible charging infrastructure. Wireless power transfer (WPT, Fig. 1.) offers a convenient method of mitigating this barrier by offering charging opportunities without the need for plugging in heavy-gauge cables [1], [2]. These cables can be a safety hazard, especially in poor weather conditions [3], [4].

WPT utilizes a stationary charging coil arrangement to produce a magnetic field which induces a voltage on a receiving coil array present on the EV. This induced voltage is rectified and used to charge the EV battery. The efficiency of a WPT system is highly dependent on the positioning of the receiver coil with respect to the transmitter [5]. As the receiver is misaligned from the magnetic center of the transmitter, the mutual inductances between the transmitter and receiver

Manuscript received February 21, 2019; revised May 30, 2019; accepted June 30, 2019. Date of publication July 10, 2019; date of current version January 7, 2020. This work was supported in part by the Natural Sciences and Engineering Research Council of Canada (NSERC). (Corresponding author: Mehanathan Pathmanathan.)

The authors are with the Edward S. Rogers Department of Electrical and Computer Engineering, University of Toronto, Toronto, ON M5S 3G4, Canada (e-mail: meha.pathmanathan@utoronto.ca; shuang.nie@mail.utoronto.ca; netan.yakop@mail.utoronto.ca; lehn@ecf.utoronto.ca).

Digital Object Identifier 10.1109/TTE.2019.2927845

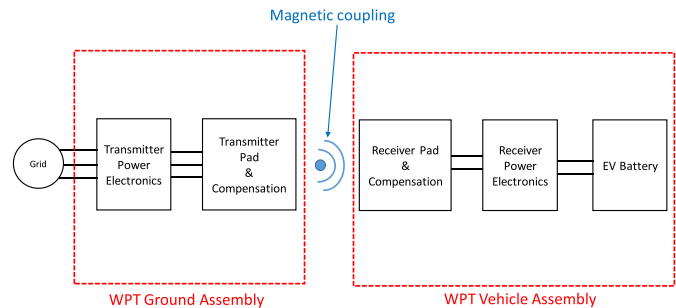


Fig. 1. Overview of a typical WPT system for EV charging.

coils degrade, and hence, higher currents are required in the transmitter coils in order to transfer a given value of power to the EV battery. These higher currents increase the copper and power electronic losses in the transmitter and eventually may reach the current limits of the transmitter, causing the charging power to be limited [5].

Early WPT systems were designed with circular pads (CPs), which utilized a simple magnetic structure [6], [7]. A downside of the CP was the low levels of magnetic coupling and poor misalignment tolerance a CP transmitter would have with a given receiver [4]. Solenoid-based transmitter coil technologies were proposed as an alternative with higher coupling factors and improved misalignment tolerance [8], [9]. However, these coil topologies suffered from a significant degradation in transmission efficiency when aluminum shielding was used for leakage flux mitigation [3].

The double-D (DD) pad was proposed as a coil topology, which combined the benefits of the CP- and solenoid-based transmitters, in that it exhibited high magnetic coupling and reduced losses due to the aluminum shielding [10]. The misalignment tolerance of the DD pad was improved by adding a third quadrature coil, forming the DD-quadrature (DDQ) topology [10]. An alternative coil topology, which exhibits similar misalignment tolerance and coupling as the DDQ while utilizing 25%–30% less copper, is the bipolar pad (BP). The BP can be driven with current sources of varying magnitude and phase in order to operate with magnetic coupling and leakage flux characteristics which are required for a given situation [11], [12]. In these studies, the BP was typically driven with the two transmitter currents in-phase to create a vertical flux pattern (suitable for a perfectly aligned CP receiver or misaligned DD receiver) or with the transmitter

currents 180° out of phase (suitable for a misaligned CP receiver or aligned DD receiver). In [25], it was found that the transmitter currents in a BP could be represented as functions of their relative gain and phase difference and it was possible to maximize system efficiency as a function of misalignment by controlling these variables. Lin *et al.* [24] stated that operating a BP transmitter in single-coil mode at extreme misalignments resulted in the lowest possible leakage flux.

Three-phase WPT transmitting coils have been proposed as an alternative to the single- and two-phase topologies discussed thus far. Initially, the work on three-phase WPT transmitters focused on dynamic charging applications for automatic guided vehicles [13], [14], light rail vehicles [15], [16], or low-power planar transformers [17]. Matsumoto *et al.* [18] proposed a static three-phase WPT technology based on a circular design. In this study, the receiver coil was also constrained to have the same magnetic structure as the three-phase transmitter. Kim *et al.* [19] presented an alternative where the three circular transmitting coils were overlapped in order to magnetically decouple them similarly to the BP. This technique ensured that each phase of the tripolar coil could be energized without impacting the control of the current driven in other phases. The work in [20] also examined the operation of this tripolar transmitter with other receivers such as the CP. An exhaustive search controller was used to derive the required magnitude and phases of the transmitter currents in the tripolar coil.

This paper presents an alternative three-phase transmitter for static WPT applications whose geometry is analogous to a three-phase, two-pole stator winding of an electrical machine. The lateral misalignment of the receiver with respect to the transmitter is used to calculate an equivalent “rotor angle.” Based on this angle, the Park transform can be used to derive direct and quadrature axis components of transmitter currents. Neglecting end effects of the three-phase wireless transmitter, direct axis transmitter current corresponds to a magnetic flux which is projected directly toward the receiver, while the quadrature axis current corresponds to a magnetic flux projected at a misalignment analogous to 90° equivalent degrees from the receiver.

Using this knowledge, it is possible to derive a transmitter current distribution which projects the generated magnetic flux toward a receiver at any lateral misalignment. This field reorientation maximizes the coil efficiency of the WPT system by minimizing the magnitude of the transmitter current vector required and hence, minimizing I^2R losses. In contrast to the method proposed by [25] used with Bipolar coils, the methodology presented in this paper allows the optimal transmitter current to be calculated as a function of the receiver position. The proposed method allows for a simplified solution methodology compared to the optimization-based technique in [30] at the expense of requiring a transmitter structure, which is designed according to a three-phase, two-pole winding.

In this paper, the proposed analysis is used to derive the required transmitter currents, compensation capacitors, and driving voltages as a function of misalignment for a WPT system using a CP receiver topology. The CP is utilized on the

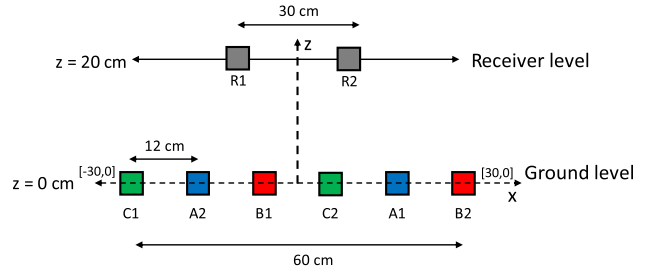


Fig. 2. Winding diagram of the four-coil WPT system.

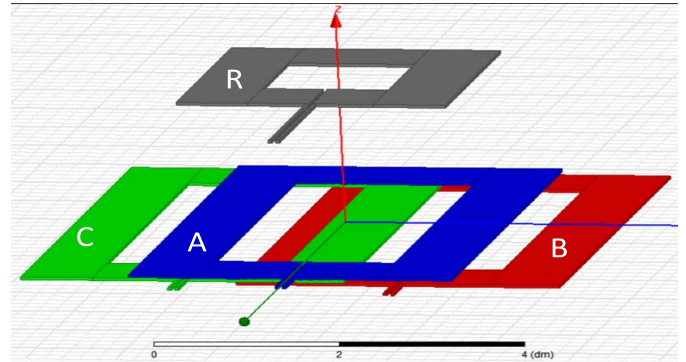


Fig. 3. Four-coil WPT system geometry.

receiver side in order to minimize the weight and complexity of the receiver mounted on the EV. The analysis is verified by simulations and experimental results showing a WPT system with a minimum coil efficiency of 90.52% at 20-cm lateral misalignment for 1-kW power transfer into a 300-V battery.

II. SYSTEM MODELING

A winding diagram of the four-coil WPT system is shown in Fig. 2. The three-phase transmitter is designed according to a three-phase, two-pole electrical machine stator winding with slots per pole per phase equal to 1 [22]. If this stator winding design is “cut and unrolled” according to the conventional procedure of linear machine design [23], the flat transmitter structure shown in Fig. 2 is obtained. Given that the required outer dimension of the transmitter was 600 mm, a pole pitch p of 120 mm is used (which corresponds to a 120° phase shift between each coil). This value of p gives rise to a width of 360 mm for each transmitter coil.

Since a rectangular transmitter coil structure was desired, the length of each individual transmitter coil was set to 600 mm, thereby giving rise to $360 \text{ mm} \times 600 \text{ mm}$ dimensions for each transmitter coil. The overall three-phase transmitter had dimensions of $600 \text{ mm} \times 600 \text{ mm}$. The receiver was set to have a CP structure and $300 \text{ mm} \times 300 \text{ mm}$ dimensions. Fig. 3 shows a constructed three-dimensional FEA model of the four-coil WPT system in ANSYS Maxwell. Sixteen turns were used for each transmitting coil, while 20 turns were used for the receiver.

The first step in deriving the required transmitter currents as a function of output power reference and receiver lateral misalignment is to convert this misalignment into an equivalent

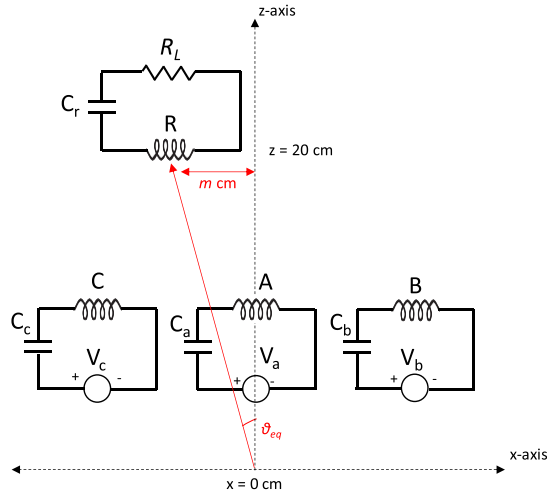


Fig. 4. Electrical equivalent circuit of the four-coil WPT system.

angle. The following expression is used for this purpose:

$$\theta_{\text{eq}} = \frac{\pi m}{3p} \quad (1)$$

where m is the lateral misalignment of the receiver with respect to the center of the transmitter, and p is the pole pitch (120 mm in the design shown in Fig. 2).

Once the equivalent angle of the receiver with respect to the transmitter is known, the relationship between the three coil currents and their direct and quadrature components is obtained from the (inverse) Park transform

$$\mathbf{I} = \sqrt{\frac{2}{3}} \begin{bmatrix} \cos(\theta_{\text{eq}}) & -\sin(\theta_{\text{eq}}) & \sqrt{2}/2 \\ \cos(\theta_{\text{eq}} - 2\pi/3) & -\sin(\theta_{\text{eq}} - 2\pi/3) & \sqrt{2}/2 \\ \cos(\theta_{\text{eq}} + 2\pi/3) & -\sin(\theta_{\text{eq}} + 2\pi/3) & \sqrt{2}/2 \end{bmatrix} \begin{bmatrix} i_d \\ i_q \\ i_0 \end{bmatrix} \quad (2)$$

where $\mathbf{I} = [I_a, I_b, I_c]^T$. Since i_d , i_q , and i_0 are real-valued and θ_{eq} is fixed for a given operating point, $I_a - I_c$ will be signed real values.

In the time domain, $I_a - I_c$ can be represented as $i_n(t) = I_n \cos(\omega t)$, where ω is the operating frequency of the WPT system in radians/second. Due to the sign differences in I_n , the transmitter currents in the time domain will either be in-phase or 180° out of phase.

It should be noted that i_d produces a flux vector which is oriented toward the receiver, whereas the quadrature component produces a flux vector oriented at 90° from the receiver. This is analogous to an electrical machine, where the d -axis current produces magnetizing flux and the q -axis current generates torque-producing flux. In contrast, i_0 produces a common mode flux which is not strongly directed at a particular lateral position. As a result, i_0 is set to zero in this paper to simplify the analysis of the three-phase transmitter currents.

An equivalent electrical circuit of the four coil WPT system is shown in Fig. 4. In this paper, series compensation capacitors will be used for both the transmitter and receiver coils [subsystems (SS) compensation]. C_a is assigned to the center, C_b to the right, and C_c to the left transmitter coils (A, B, and C, respectively). Each of the transmitter coils is driven by

an independent voltage source, V_a , V_b , and V_c for coils (A, B, and C, respectively).

In the analytical model, the receiver is connected to the series compensation capacitor C_r and an equivalent load resistance R_L .

The value of R_L is derived from the first harmonic approximation of a voltage-doubling rectifier with dc voltage load V_{dc} and is given by

$$R_L = \frac{2V_{\text{dc}}^2}{\pi^2 P_o} \quad (3)$$

where P_o is the desired output power level.

A. Current Reference Calculation

The electrical circuit shown in Fig. 4 can be analyzed in the following fashion:

$$\begin{bmatrix} V_a \\ V_b \\ V_c \\ 0 \end{bmatrix} = \begin{bmatrix} Z_{sA} & j\omega L_{AB} & j\omega L_{AC} & j\omega L_{AR} \\ j\omega L_{BA} & Z_{sB} & j\omega L_{BC} & j\omega L_{BR} \\ j\omega L_{CA} & j\omega L_{CB} & Z_{sC} & j\omega L_{CR} \\ j\omega L_{RA} & j\omega L_{RB} & j\omega L_{RC} & Z_{sR} \end{bmatrix} \begin{bmatrix} I_a \\ I_b \\ I_c \\ I_R \end{bmatrix} \quad (4)$$

The impedance Z_{sN} is defined as

$$Z_{sN} = j\omega L_{nn} - \frac{j}{\omega C_n} + R_n. \quad (5)$$

For coils A, B, and C, the resistance in this equation is their own intrinsic resistance. For coil R, this resistance is equal to the sum of this intrinsic resistance with R_L .

In this paper, the value of C_r is calculated to compensate for the self-inductance of the receiver

$$C_r = \frac{1}{\omega^2 L_{RR}}. \quad (6)$$

The receiver current can then be calculated from (4) as follows:

$$I_R = \frac{-j\omega(L_{AR}I_a + L_{BR}I_b + L_{CR}I_c)}{R_L + R_R} \quad (7)$$

where R_R is the resistance of the receiver coil. Note that the receiver current is purely imaginary, indicating that there will be a 90° phase shift between the transmitter and receiver currents. If $i_q = 0$ and $i_0 = 0$, the inverse park transform can be used to derive the receiver current as a function of i_d (8), as shown at the bottom of the next page.

Since $P_o = |I_R|^2 R_L$, the required i_d for given output power and misalignment is (9), as shown at the bottom of the next page.

Equation (2) can then be used to calculate the required current magnitude in each phase.

The required compensation capacitors are obtained by solving the first three rows of (4) for the capacitance values, which result in zero imaginary component for the transmitter voltages (thereby resulting in unity transmitter power factor)

$$C_a = \frac{I_a}{\omega^2(L_{AA}I_a + L_{AB}I_b + L_{AC}I_c)} \quad (10)$$

$$C_b = \frac{I_b}{\omega^2(L_{BA}I_a + L_{BB}I_b + L_{BC}I_c)} \quad (11)$$

$$C_c = \frac{I_c}{\omega^2(L_{CA}I_a + L_{CB}I_b + L_{CC}I_c)}. \quad (12)$$

Based on these capacitance values and the known i_d reference for a given power and misalignment, the required transmitter voltages can be calculated as

$$V_a = I_a R_a + \frac{\omega^2 L_{AR} (L_{AR} I_a + L_{BR} I_b + L_{CR} I_c)}{R_r + R_L} \quad (13)$$

$$V_b = I_b R_b + \frac{\omega^2 L_{BR} (L_{AR} I_a + L_{BR} I_b + L_{CR} I_c)}{R_r + R_L} \quad (14)$$

$$V_c = I_c R_c + \frac{\omega^2 L_{CR} (L_{AR} I_a + L_{BR} I_b + L_{CR} I_c)}{R_r + R_L}. \quad (15)$$

The total copper losses of the WPT system are given by the following equation:

$$P_l = |I_a|^2 R_a + |I_b|^2 R_b + |I_c|^2 R_c + |I_r|^2 R_r. \quad (16)$$

The calculated efficiency is then obtained by

$$\eta = \frac{P_o}{P_o + P_l} \quad (17)$$

where $P_o = |I_r|^2 R_L$.

B. Calculated Performance

A finite element model was constructed in ANSYS Maxwell based on the geometry shown in Fig. 3. This model was used to compute the self and mutual inductances of the four-coil WPT system. The receiver coil resistance (R_r) was 110 m Ω , while the transmitter coil resistances ($R_a - R_c$) were 200 m Ω .

At perfect receiver alignment, the following inductance matrix is obtained:

$$\mathbf{L} = \begin{bmatrix} 223 \mu\text{H} & 85 \mu\text{H} & 87 \mu\text{H} & 14.8 \mu\text{H} \\ 85 \mu\text{H} & 224 \mu\text{H} & -5.7 \mu\text{H} & -11.4 \mu\text{H} \\ 87 \mu\text{H} & -5.7 \mu\text{H} & 224 \mu\text{H} & -10.8 \mu\text{H} \\ 14.8 \mu\text{H} & -11.4 \mu\text{H} & -10.8 \mu\text{H} & 129 \mu\text{H} \end{bmatrix}.$$

The signs of mutual inductance are determined based on a positive coil current defined as flowing into terminal $N1$ and out of terminal $N2$ and induced voltage being measured across terminals $N1-N2$, where N represents the coil subscript shown in Fig. 2 (A, B, C, or R). A negative mutual inductance value indicates that a positive injection of current into one coil will induce a negative voltage measured from terminal 1 to 2 of the coupled coil.

As the receiver is misaligned from the center of the transmitting coil, the mutual inductances between the transmitting coil and the receiver begin to change. Fig. 5 shows this variation as the receiver is moved from the center of the transmitting coil toward the right side of Fig. 3 (i.e., toward coil B).

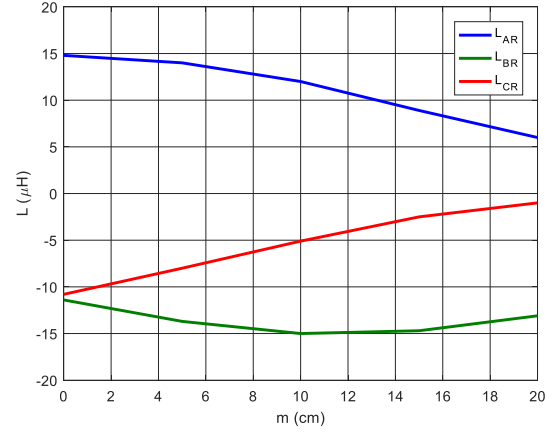


Fig. 5. Variation of transmitter-receiver mutual inductance with receiver misalignment.

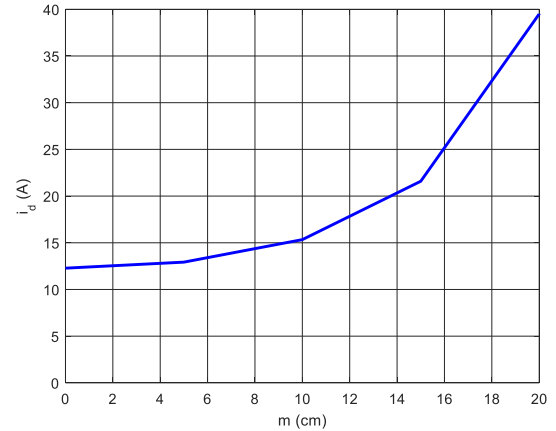


Fig. 6. Required i_d reference as a function of misalignment for 3.3-kW power transfer.

Based on these inductances, the required d -axis current reference for 3.3 kW output power can be calculated using (1), (3), and (9), as shown in Fig. 6. Once the required i_d is known and given that i_q and i_0 are set to zero, the required current in each transmitter coil can be given by (2). Fig. 7 shows the calculated current magnitude values in each coil as a function of receiver misalignment. The phase value of each current is zero; thus, due to the positive or negative signs in the time domain, each current waveform is either in-phase or 180° out of phase. This configuration ensures that the requirement of $i_0 = 0$ is respected.

$$I_R = \frac{-\sqrt{2} j \omega i_d (L_{AR} \cos(\theta_{eq}) + L_{BR} (\theta_{eq} - \frac{2\pi}{3}) + L_{CR} (\theta_{eq} + \frac{2\pi}{3}))}{(\sqrt{3}(R_L + R_r))} \quad (8)$$

$$i_d = \sqrt{\frac{3P_o(R_L + R_r)^2}{2\omega^2 R_L (L_{AR} \cos \theta_{eq} + L_{BR} \cos (\theta_{eq} - \frac{2\pi}{3}) + L_{CR} \cos (\theta_{eq} + \frac{2\pi}{3}))^2}} \quad (9)$$

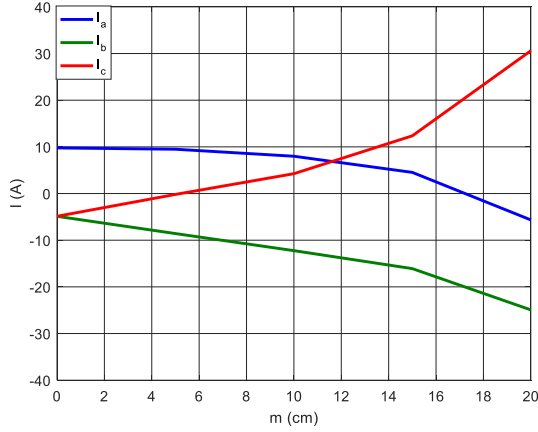


Fig. 7. Required transmitter coil current magnitude values as a function of misalignment for 3.3-kW power transfer.

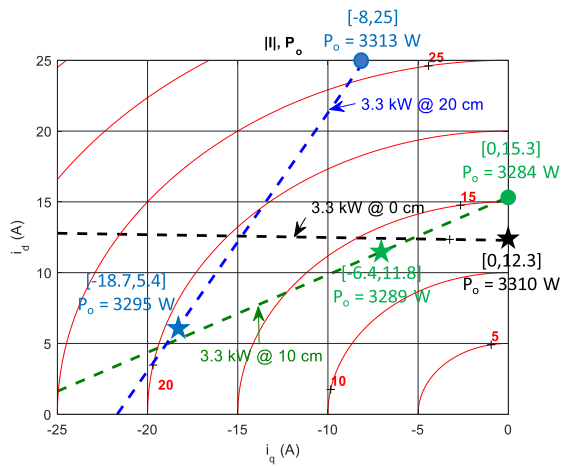


Fig. 8. Dq current trajectories for 3.3-kW output power at misalignments of 0, 10, and 20 cm.

C. Investigation of i_q Injection

Ideally (with an infinitely long stator), injecting i_q should not produce any flux aligned with the receiver. However, due to the end effects of the three-coil transmitter, it is envisaged that there may be solutions resulting in higher efficiency if an injection of i_q was used.

Fig. 8 shows contour plots of transmitter coil magnitude $|I| = (i_d^2 + i_q^2)^{1/2}$ as i_d is varied from 0 to 25 A, and i_q is varied from 0 to -25 A. On the same plot, three dashed lines are shown providing the i_d and i_q values, which result in an output power of 3.3 kW at 0 cm (black), 10 cm (green), and 20 cm (blue) misalignment.

The dashed line corresponding to 3.3-kW power transfer at 0-cm misalignment is horizontal: this indicates that there is no benefit in injecting i_q when the receiver is perfectly aligned with the receiver.

TABLE I
CURRENT VALUES FOR 3.3-kW POWER TRANSFER

m (cm)	i_d (A)	i_q (A)	I_a (A)	I_b (A)	I_c (A)
0	12.3	0	10	-5	-5
5	12.2	-3	10	-6.8	-3.3
10	11.8	-6.4	10.2	-8.6	-1.6
15	10.24	-11.8	11.47	-10.6	-0.97
20	5.4	-18.7	14.3	-13.2	-1.1

In contrast, the dashed lines corresponding to 3.3-kW transfer with 10- and 20-cm misalignment have slopes of increasing magnitude. In fact, observation of the dashed line corresponding to 3.3-kW power transfer at 10-cm misalignment shows that only injecting i_d will require a current magnitude of 15.3 A to transfer approximately 3.3 kW. However, injecting an i_q component of -6.4 A will reduce the required i_d for 3.3 kW transfer to be 11.8 A, resulting in a current magnitude of $|I| = 13.4$ A. Since the transmitter copper losses are proportional to the current magnitude squared, the injection of i_q clearly results in an efficiency improvement at 10-cm misalignment.

The impact of i_q injection is even greater at a misalignment of 20 cm, which can be observed by the steeper blue dashed curve compared to the green one. In all the observed misalignment cases, the trajectory for constant power operation is a straight line. We can obtain the q -axis intercept of this line by solving (9) (which is now called as i_{d0}). The d -axis intercept can be found by starting from (7) then applying the inverse Park transform with the value of i_d and i_0 set to zero. The resulting equation is given in (18), as shown at the bottom of the page.

Once the values of both i_{d0} and i_{q0} are known, the trajectory of i_d and i_q , which results in a required value of output power, can be obtained by solving for the equation of a straight line

$$i_d = i_{d0} \left(1 - \frac{i_q}{i_{q0}} \right). \quad (19)$$

Given the set of i_d and i_q , which result in the desired output power, are obtained from (19), the values of these variables can be solved numerically to minimize $|I|$ (thereby minimizing copper losses).

Table I shows the values of i_d and i_q , which result in the lowest $|I|$ (for 0–15 cm) for the required 3.3-kW output power and q -axis current values, were selected in order to provide a nonnegative value for C_c (which would occur if the dq currents for different values of misalignment, along with the resulting three-phase coil current magnitudes. For the 20-cm case, the d for minimum $|I|$ was used). Once the currents are known, (10)–(15) can be used to calculate the required voltage and

$$i_{q0} = - \sqrt{\frac{3P_o(R_L + R_d)^2}{2\omega^2 R_L (L_{AR} \sin \theta_{eq} + L_{BR} \sin (\theta_{eq} - \frac{2\pi}{3}) + L_{CR} \sin (\theta_{eq} + \frac{2\pi}{3}))^2}} \quad (18)$$

TABLE II
VOLTAGE AND CAPACITANCE FOR 3.3-kW POWER TRANSFER

m (cm)	V_a (V)	V_b (V)	V_c (V)	C_a (nF)	C_b (nF)	C_c (nF)
0	196.1	-150.3	-142.4	11.3	8.7	8.7
5	185.7	-180.8	-105.4	11.3	9.9	7
10	159.4	-198	-66.9	11.3	10.8	4.4
15	119.6	-195	-32.9	11.3	11.1	2.5
20	82.6	-174.9	-13.4	11.3	11.1	2.5

TABLE III
VOLTAGES AND POWER FACTOR WITHOUT RETUNING

m (cm)	pf_A	pf_B	pf_C	$ V_a $ (V)	$ V_b $ (V)	$ V_c $ (V)
0	1	1	1	196.1	150.3	142.4
5	1	0.55	0.75	185.7	198	246
10	1	0.2	0.52	159.4	341	382
15	1	0.07	0.39	119.6	466	493
20	1	0.02	0.29	82.6	580	591

series compensation capacitor values for the transmitting coils which are shown in Table II.

It should be noted that the value of I_b increases as a function of misalignment, while I_c reduces. This is intuitive since the definition of misalignment in this paper is that the receiver is moving laterally toward the coil B (driven by I_b) and away from the coil C (driven by I_c).

The reduced transmitter current magnitudes which arise due to i_q injection ultimately will result in a reduction of transmitter copper loss. As a result, i_q injection is used in the remainder of this paper.

D. Switched Capacitor Justification and Implementation

A question that could be raised is the impact of using fixed capacitors for C_a and C_b rather than the variable values in Table II. Table III shows the calculated values of power factor for phases B and C in addition to the required transmitter voltage magnitudes, when C_a and C_b were fixed to their perfect alignment value (8.7 nF). The largest transmitter voltage for the nonretuning case in Table III is 2.98 times greater than the largest voltage obtained with capacitor retuning in Table II.

This increase in voltage will result in a greater required voltage rating for the transmitter power electronic converter. Moreover, the increased dc bus voltage needed will result in increased switching losses, thereby driving down the system efficiency. For these reasons, a switched-capacitor based approach is proposed for C_b and C_c .

The experimental work presented in this paper depends on the off-line retuning of capacitors to ensure correct values of C_b and C_c are obtained. A commercially deployable variant of this method could be achieved by using receiver position detection methods based on radio-frequency identification sensors [26] or transmitter-side electrical information [27]. The required variable transmitter capacitances can be implemented via capacitor banks, which allow different capacitance values to be synthesized. The desired capacitor values can be obtained

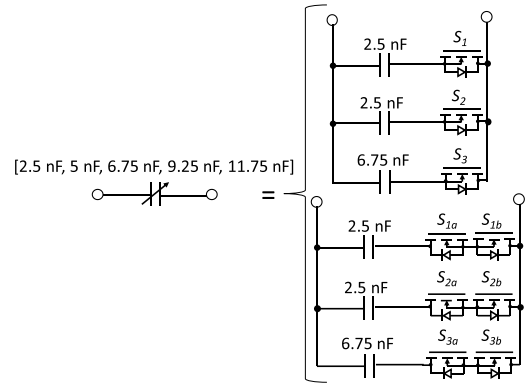


Fig. 9. Switched capacitor implementation using ac switches comprised of single MOSFETs for ZCS [28] or anti-series MOSFETs for ZVS [29].

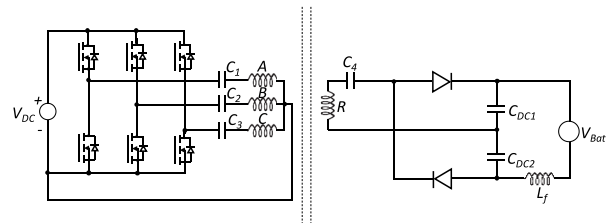


Fig. 10. Power electronic topology to be used with the four-coil WPT system.

by utilizing semiconductors as selector switches. The series capacitor-insulated gate bipolar transistor (IGBT) configuration in [28] can be adopted for this application (replacing the IGBT with a MOSFET to reduce losses). When the gate signal of the MOSFET is set to zero, the MOSFET will turn off with zero current switching as the resonant current attempts to reverse through the anti-parallel diode. This results in a condition corresponding to state 5 in [28] where the capacitor remains charged but will not conduct any current until the MOSFET is gated on again.

An alternative method is to use anti-series MOSFETs as capacitance selector switches [29]. In comparison to the method presented in [28], the MOSFETs can be turned off at the capacitor voltage zero-crossing, meaning that no stored dc voltage will be present on a capacitor while it is not inserted into the circuit. This will result in lower voltage stress across the selector MOSFETs compared to the method in [28]. The downside of using anti-series MOSFETs is that a more complex gate driver is required, and precise sensing is needed to ensure zero voltage switching is achieved.

Fig. 9 shows examples of how the methods of [28] and [29] can be used to synthesize capacitance values which are close to C_b and C_c (2.5, 5, 6.75, 9.25, and 11.75 nF) in Table II.

III. SIMULATION MODEL

Fig. 10 shows the power electronic topology, which was used to realize the four-coil WPT system. On the transmitter side, a three-phase, the two-level inverter is used. The three transmitter coils are star-connected, and the resulting neutral point is connected to the negative terminal of the inverter dc bus. This technique allows the three transmitter coils to be independently driven by each phase leg of the inverter.

TABLE IV
SIMULATION MODEL PARAMETERS

Parameter	Description	Value
V_{bat}	Battery voltage	300 V
L_f	Voltage doubler filter inductance	2.2 μ H
C_{dc}	Voltage doubler DC capacitance	40 μ F
R_r-R_c	Transmitter coil resistances	200 m Ω
R_r	Receiver coil resistance	110 m Ω
f_s	Inverter switching frequency	85 kHz

In addition, the series compensation capacitors $C_a - C_c$ act as coupling capacitors, which remove the dc component present on each transmitter coil voltage, when this topology and modulation scheme is used. The fundamental component of the transmitter voltage can be derived from the Fourier series decomposition and is given in (20)–(22), where d is the duty cycle of a phase leg in the two-level inverter

$$a_1 = \frac{V_{dc}}{\pi} \sin(2\pi d) \quad (20)$$

$$b_1 = \frac{V_{dc}}{\pi} [\cos(2\pi d) - 1] \quad (21)$$

$$V_1(t) = a_1 \cos(\omega t) + b_1 \sin(\omega t). \quad (22)$$

A voltage-doubling rectifier is used on the receiver side in conjunction with series compensation capacitor C_r . On the dc side of this rectifier, a filter inductor L_f is used to filter the ripple component of the battery current, when combined with the dc capacitors C_{dc1} and C_{dc2} . Values of 40 μ F for the capacitors and 2.2 μ H for the inductor were used to filter the 170-kHz dc current ripple component (second harmonic of the operating frequency).

A simulation model was constructed in Simulink in order to verify the current references and compensation capacitors derived for different alignments in Section II-C, in addition to the power electronic topology and modulation scheme introduced in this section. The self and mutual inductance values of the coils were the same as those given in Section II-B, while the compensation capacitor values were the same as those shown in Table II. The remaining parameters in the model, which were held constant as a function of misalignment are listed in Table IV.

It is intended that the simulation model should deliver the same fundamental transmitter voltages listed in Table II as a function of misalignment. In order to minimize the harmonic distortion of the modulated transmitter voltage waveforms, the inverter dc-link voltage V_{dc} was controlled in order to ensure that at least one of the three legs of the transmitter inverter would operate at a duty cycle of 50%. This V_{dc} is calculated using the following equation:

$$V_{dc} = \frac{\max(V_{n_{pk}}) \times \pi}{2}, \quad n \in 1, 2, 3. \quad (23)$$

The value given by (21) is also the minimum required inverter dc-link voltage. The required values of V_{dc} for receiver misalignments in the range 0–20 cm are provided in Table V, together with the required duty cycles and phase shifts of

TABLE V
CALCULATED DUTY CYCLE AND PHASE SHIFT VALUES FOR EACH LEG

m (cm)	V_{dc} (V)	d_1 (%)	d_2 (%)	d_3 (%)	α_1 ($^\circ$)	α_2 ($^\circ$)	α_3 ($^\circ$)
0	436.4	50	29	27	0	180	180
5	412.8	50	50	20	0	180	180
10	439.9	31	50	12	0	180	180
15	433.2	22	50	6	0	180	180
20	388.5	17	50	3	0	180	180

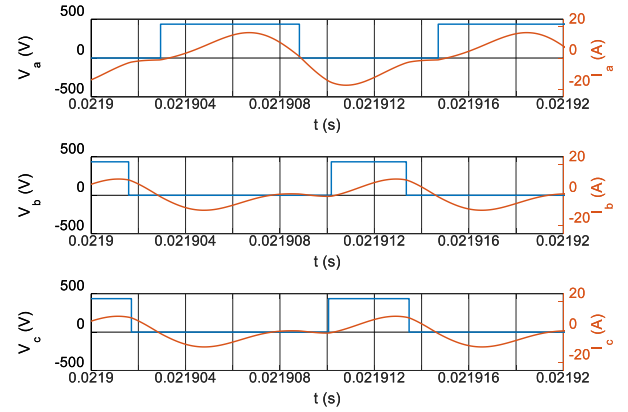


Fig. 11. Simulated transmitter voltage and current waveforms for 3.3-kW power transfer at perfect alignment ($m = 0$).

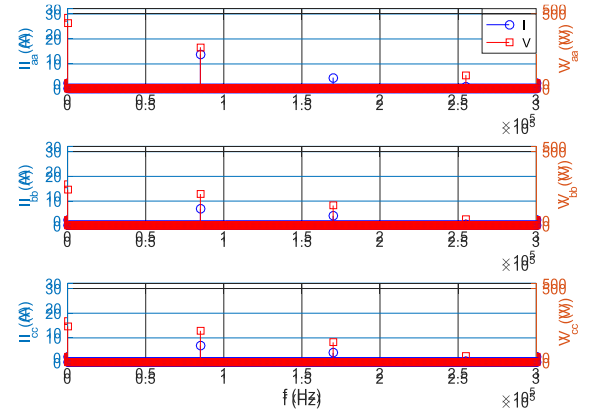


Fig. 12. Frequency spectra of the simulated transmitter voltages and currents for 3.3-kW power transfer at perfect alignment ($m = 0$).

each leg of the three-phase inverter. This table also shows the required phase angle α , which must be applied to the gate drive signal of each inverter leg to ensure the voltages are either in phase or 180° out of phase, as given in Table II.

Fig. 11 shows the simulated phase voltage and current values at perfect alignment ($m = 0$). While significant second and third harmonic components exist in the transmitter current waveforms, no dc current component exists. This indicates that the series compensation capacitors have removed the dc voltage bias, as intended. The frequency spectra of the transmitter voltages and currents shown in Fig. 12 show this: while there is a clear 0-Hz component in the voltage spectrum, it is absent from the current spectrum. The elimination of dc bias in the transmitter currents is essential for future

TABLE VI
SIMULATED TRANSMITTER FUNDAMENTAL RMS COMPONENTS

m (cm)	V_{a_1} (V)	V_{b_1} (V)	V_{c_1} (V)	I_{a_1} (A)	I_{b_1} (A)	I_{c_1} (A)
0	196.4	-155.2	-147.4	10.04	-5.02	-5.02
5	185.8	-185.8	-109.3	10.07	-6.76	-3.31
10	163.7	-198	-72.9	10.22	-8.6	-1.62
15	124.3	-195	-36.5	11.49	-10.58	-0.90
20	89	-174.9	-16.5	14.33	-13.21	-1.13

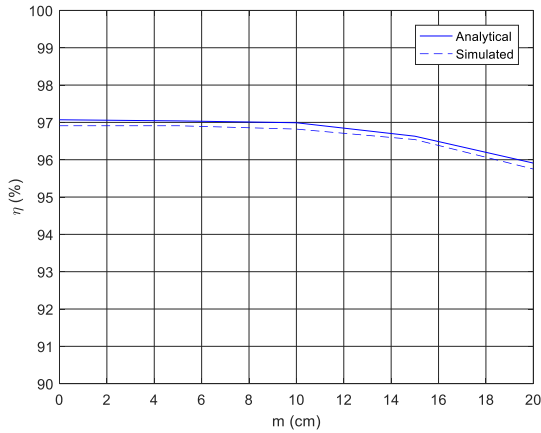


Fig. 13. Comparison of calculated (using first harmonic analysis) and simulated efficiency (from Simulink model) for a power transfer of 3.3 kW into a 300-V battery.

transmitter designs, which include magnetic material since this bias current can be a cause of magnetic saturation.

The fundamental rms components of transmitter voltage and current for a range of misalignment between 0 and 20 cm are shown in Table VI. Comparing these results with the voltage and current references derived based on first harmonic analysis in Tables II and III validates the efficacy of the selected power electronic converter topology and modulation method.

Fig. 13 shows a comparison of the calculated (17) and simulated (using the Simulink model used in this section) coil efficiencies as a function of misalignment for an output power of 3.3 kW. The reduction in simulated efficiency is due to the first harmonic approximation (Section II) neglecting the higher order harmonics in the transmitter and receiver currents which arise due to the choice of power electronic converter topology and modulation strategy.

Fig. 14 shows the magnetic flux density vectors calculated by two-dimensional finite-element simulations conducted in ANSYS Maxwell for misalignments of 0, 10, and 20 cm. The coils were excited with corresponding current values given in Table VI for these simulations. The flux density plots show that the strongest vertical component of flux density “shifts” toward the right for the 10- and 20-cm misaligned cases. At 20 cm, the strongest vertical flux density component cannot be shifted laterally all the way toward the receiver using the transmitter current distribution from Table VI. This is the reason for the efficiency degradation from 97% at 10 cm to 96% at 20 cm, which is shown in Fig. 13.

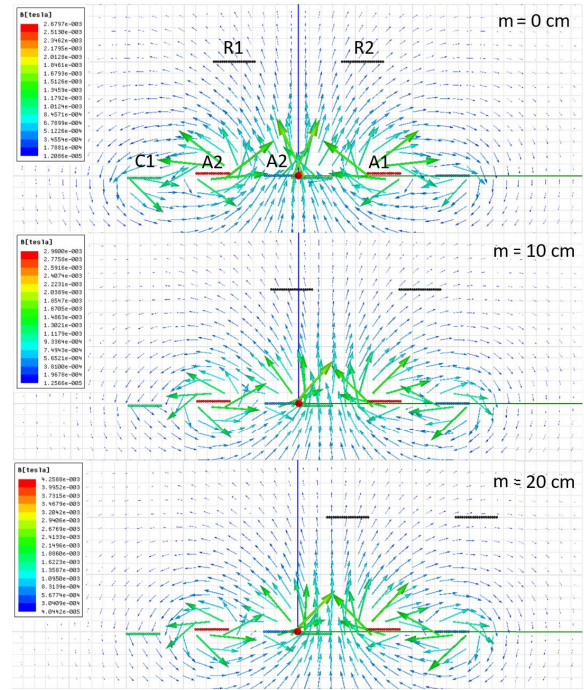


Fig. 14. Magnetic flux density vector graph from ANSYS Maxwell, for misalignments of 0 cm (top), 10 cm (middle), and 20 cm (bottom), where transmitter excitation currents at each misalignment were obtained from Table VI.

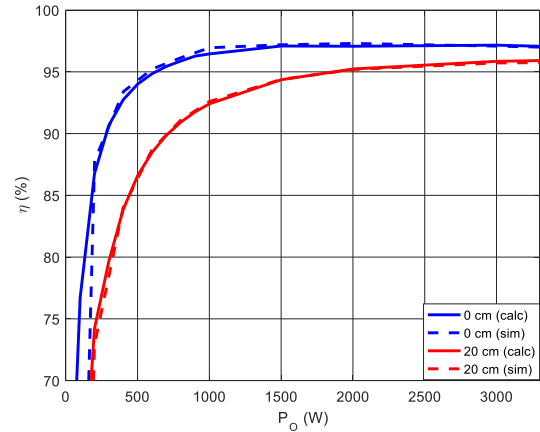


Fig. 15. Comparison of calculated (using first harmonic analysis) and simulated (from Simulink model) efficiency as a function of output power when a 300-V battery with a receiver-side voltage-doubling rectifier was used.

Calculated (17) and simulated (from Simulink model) results of coil efficiency as a function of output power for misalignments of 0 and 20 cm are shown in Fig. 15. For both cases, the efficiency is lower for lower power transfer levels. The reason behind this can be understood by realizing that the transmitter copper losses are constant as a function of output power when a battery load with rectifier (voltage doubler or conventional) is used on the receiver side. In contrast, the receiver copper losses increase as a function of output power.

In the four-coil WPT system investigated in this paper, the transmitter copper losses are greater than the receiver copper

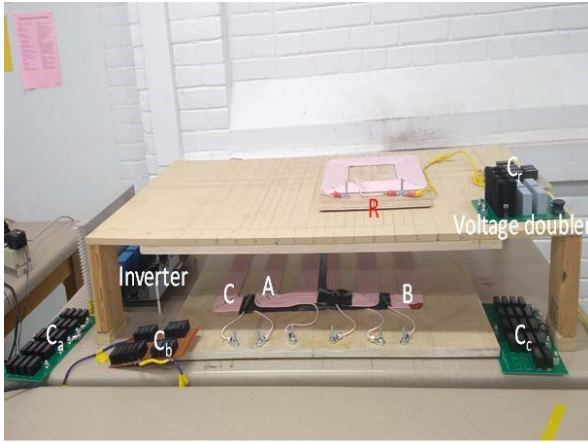


Fig. 16. Experimental setup built in the laboratory.

TABLE VII
REQUIRED TRANSMITTER CURRENT AND VOLTAGE
FOR 1-kW POWER TRANSFER

m (cm)	i_d (A)	i_q (A)	V_a (V)	V_b (V)	V_c (V)
0	12.3	0	94.82	-75.86	-74.66
5	12.2	-3	87.74	-87.74	-59.51
10	11.8	-6.4	80	-90.59	-49.62
15	10.24	-11.28	64.63	-87.96	-37.32
20	5.356	-18.74	49.85	-76.93	-26.55

losses due to the higher resistance of the transmitter coils and the higher number of transmitter coils with respect to receiver coils. Thus, a significant efficiency degradation is noted at low output power values since the transmitter copper losses become significant when compared to the output power.

IV. EXPERIMENTAL SETUP

As shown in Fig. 16, a 1-kW experimental prototype of the WPT system was constructed in order to verify the proposed method of deriving transmitter currents as a function of misalignment. The transmitter and receiver coils were constructed using NELD1100 litz wire from New England Wire Technologies, while a high-frequency inverter utilizing Cree C2M0025120D SiC MOSFETs was used for the transmitter power electronics. The receiver-side voltage-doubling rectifier was developed using Cree C4D2012A SiC Schottky diodes. The compensation capacitors were deployed by forming matrices of series and parallel Elcon 5PT capacitors in order to achieve the required capacitor voltage and current ratings. All measured values shown in this section were obtained using a Hioki PW6001 power analyzer.

Table VII shows the required transmitter d and q -axis current references and corresponding phase voltages as a function of receiver misalignment. It should be noted that the voltage values in Table VII are the true rms values (including all harmonic components).

Table VIII shows the values of transmitter coil compensation capacitors C_a , C_b , and C_c , which were calculated according to (10)–(12) based on the current references in Table VI,

TABLE VIII
DESIRED AND ACTUAL TRANSMITTER COMPENSATION CAPACITORS

m (cm)	C_a (nF)	C_b (nF)	C_c (nF)	C_{ap} (nF)	C_{bp} (nF)	C_{cp} (nF)	f_t (kHz)
0	11.35	8.77	8.68	11.75	9.25	9.25	83.5
5	11.35	9.92	7.01	11.75	9.25	6.75	85
10	11.35	10.75	4.363	11.75	11.75	5	83
15	11.35	11.07	2.5	11.75	11.75	2.5	83.5
20	11.35	11.07	2.5	11.75	11.75	2.5	83

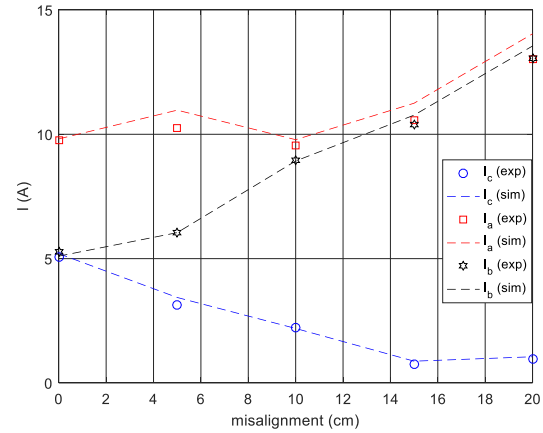


Fig. 17. Comparison of simulated and experimental transmitter current rms values as a function of receiver misalignment for 1-kW power transfer to a 300-V battery load.

and the mutual inductance variation is shown in Fig. 5. Due to limitations in available capacitors, it was only possible to synthesize transmitter capacitors of 2.5, 5, 7.5, 6.75, 8.25, and 11.75 nF. As a result, the closest capacitance value to the calculated required capacitance was used in experiments.

These were labeled as $C_{ap} - C_{cp}$. The ideal required receiver side capacitance at a frequency of 85 kHz was calculated from (6) to be 26.4 nF. The closest possible value of capacitance which could be created was 27.5 nF, which was used in all experimental results.

Due to the nonideal capacitor values which were used, the inverter switching frequency had to be slightly modified from the nominal value of 85 kHz at all misalignments apart from 5 cm. These changes were required in order to compensate for the differences between the desired and actual reactive power values, which were supplied by the compensation capacitors. It should be noted, however, that the required level of frequency tuning was well within the range of 81.38 to 90 kHz which is specified by SAE recommended practice J2954 [21].

Fig. 17 shows a comparison of the simulated and experimental rms transmitter current values as a function of misalignment for 1-kW power transfer. The required transmitter current references were calculated according to the values of i_d and i_q provided in Table VII. As desired, when the receiver is misaligned toward the right (toward coil “B” and away from “C”), the current in coil C is reduced while the current in coil B is increased.

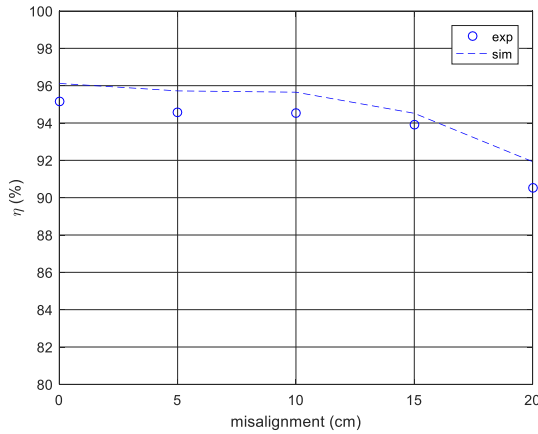


Fig. 18. Comparison of simulated and experimental coil efficiency as a function of misalignment for 1-kW power transfer into a 300-V battery load.

The coil efficiency of the four-coil WPT system is plotted as a function of receiver misalignment for a power transfer of 1 kW into a 300-V battery is shown in Fig. 18. A peak measured efficiency of 95.17% was obtained at perfect alignment, which degraded to a value of 90.52% at a misalignment of 20 cm. SAE J2954 specifies a minimum required grid to battery efficiency of 80% at a lateral misalignment of 7.5 cm. The measured coil efficiency at 10 cm is 94.53%, indicating that the proposed design should comfortably meet the SAE specifications even when power electronic losses are considered.

The simulated coil efficiency shown in Fig. 18 includes ESR losses of the compensation capacitors used in the experimental system estimated from datasheet values, in addition to the transmitter coil resistances. The error between simulated and experimental efficiency is less than 1.5% across all alignments. The discrepancy is due to unmodelled losses in the PCB traces and solder contact points of the capacitor arrays, along with wiring resistances.

Comparison of the simulated efficiency shown in Fig. 18 (for 1-kW power transfer) with the simulated curve in Fig. 13 shows a significant degradation from 95.8% to 91.9% at 20-cm misalignment. The reason for this can be understood by referring to Fig. 15, and the discussion in the previous section which explained that the required transmitter current in order to induce enough receiver voltage for power transfer with a rectifier load ultimately resulted in a significant efficiency degradation at low power values, especially for the misaligned case.

Fig. 19 shows the distribution of measured transmitter coil powers for 1-kW power transfer at the different receiver alignments. At perfect alignment, most of the power is transferred from coil A, while the remainder is almost equally distributed between coils B and C. As the receiver is misaligned toward coil B, the power transferred by coil C is reduced and eventually becomes zero at 15-cm misalignment. For the 20-cm misalignment case, most of the power is transmitted by coil B.

Fig. 20 shows the simulated waveforms of the currents and voltages for 1-kW power transfer at perfect receiver alignment. From the waveforms, it is apparent that the compensation

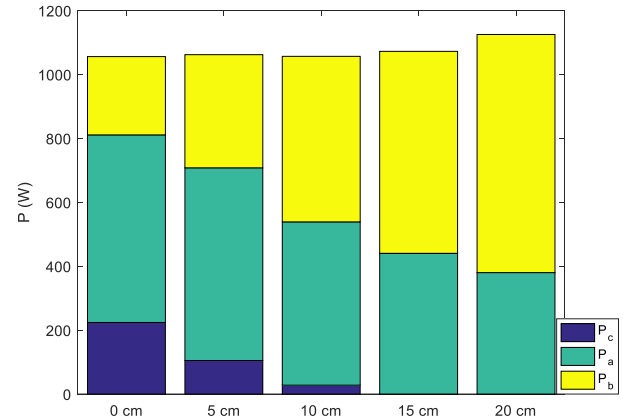


Fig. 19. Measured transmitter coil powers as a function of misalignment, for 1-kW power transfer.

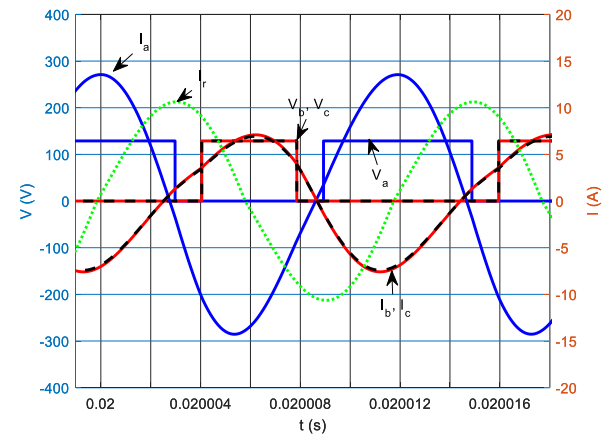


Fig. 20. Simulated waveforms for 1 kW of power transfer at 0-cm misalignment.

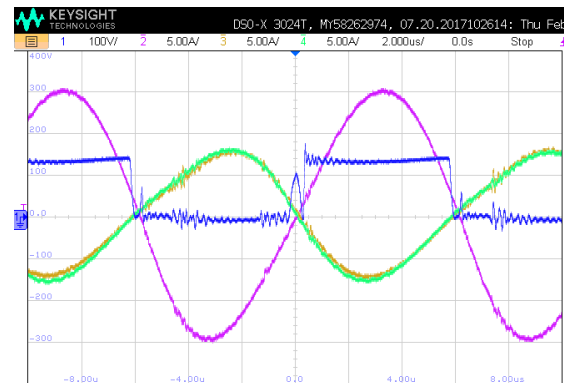


Fig. 21. Experimental waveforms of inverter phase "A" voltage (channel 1), phase "A" current (channel 2), phase "C" current (channel 3), and phase "B" current (channel 4) at a misalignment of 0 cm.

capacitor selection results in virtually no phase shift between the current waveforms and the voltage pulses. This is verified by the experimental waveforms of the same operating condition in Fig. 21. The experimental waveform only shows the

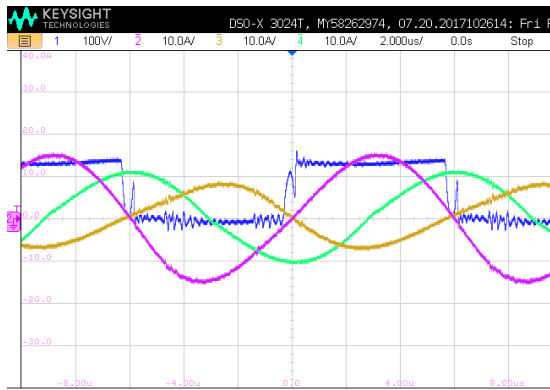


Fig. 22. Experimental waveforms of inverter phase “A” voltage (channel 1), phase “A” current (channel 2), phase “C” current (channel 3), and receiver current (channel 4) at 0-cm misalignment.

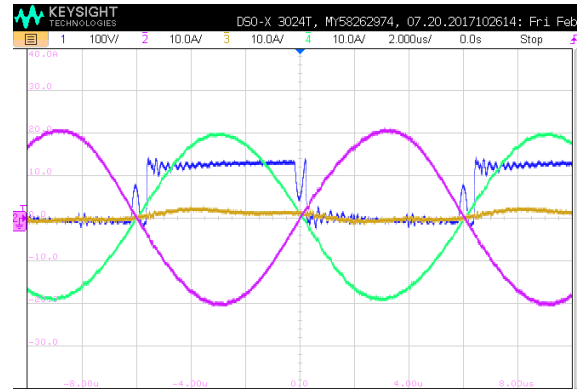


Fig. 24. Experimental waveforms of inverter phase “B” voltage (channel 1), phase “A” current (channel 2), phase “C” current (channel 3), and phase “B” current (channel 4) at a misalignment of 20 cm.

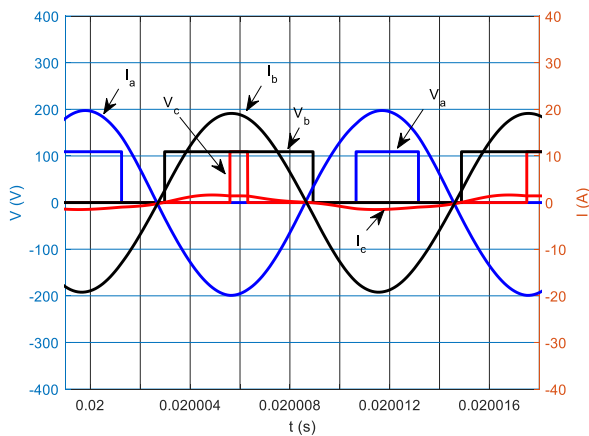


Fig. 23. Simulated waveforms for 1 kW of power transfer at 20-cm misalignment.

voltage V_a (applied to coil A) since the oscilloscope only had four channels.

The experimental waveforms in Fig. 22 show the measured waveforms at perfect alignment again, but with the receiver current shown instead of phase “B” current. A 90° phase difference is present between the receiver current and the phase “A” current both in the experimental waveforms in Fig. 22 and the simulation in Fig. 12. It is apparent from these that the receiver self-compensation method of (6) and (7) has been correctly applied since a phase shift of 90° is presented between I_a and I_r .

The simulated waveforms for 20-cm misalignment are shown in Fig. 23. Comparing with Fig. 20, the current magnitude in coil B (I_b) has increased, while the current in coil “C” (I_c) has decreased significantly. Once again, the phase shift between the current waveforms and voltage pulses are near zero indicating the success of the chosen compensation strategy. The experimental waveforms for this case are shown in Fig. 24 and have a close correspondence with the simulated values. Once again, due to the limitation of oscilloscope channels, only V_b was shown (voltage applied to coil “B”).

V. CONCLUSION

This paper presented the design of a three-phase WPT transmitter based on a three-phase two-pole electrical machine stator. Due to this design, it was possible to express the transmitter currents in terms of direct and quadrature axis components for a given receiver misalignment.

A method of calculating the required series compensation capacitances and transmitter voltages was presented for given direct and quadrature current references. A transmitter power electronic converter topology based on a three-phase inverter modulated in half-bridge mode was used in order to minimize the required power electronic switches needed to drive the three-phase WPT transmitter. A voltage-doubling rectifier was used to connect the receiver to a battery.

The performance of this design was verified by simulations at a power transfer level of 3.3 kW, and experimental results on a 1-kW prototype. The measured coil efficiency was 95.17% at perfect alignment, which degraded to 90.52% at a misalignment of 20 cm.

Future work in this area includes the development of a sensorless receiver position sensing algorithm and a closed loop control algorithm, which allows for the real-time computation of inverter duty cycle and phase shift parameters along with dynamic retuning of transmitter compensation capacitors as a function of receiver misalignment.

REFERENCES

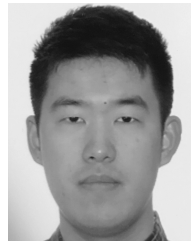
- [1] G. A. Covic and J. T. Boys, “Modern trends in inductive power transfer for transportation applications,” *IEEE J. Emerg. Sel. Topics Power Electron.*, vol. 1, no. 1, pp. 28–41, Mar. 2013.
- [2] G. A. Covic and J. T. Boys, “Inductive power transfer,” *Proc. IEEE*, vol. 101, no. 6, pp. 1276–1289, Jun. 2013.
- [3] D. Patil, M. K. McDonough, J. M. Miller, B. Fahimi, and P. T. Balsara, “Wireless power transfer for vehicular applications: Overview and challenges,” *IEEE Trans. Transport. Electric.*, vol. 4, no. 1, pp. 3–37, Mar. 2018.
- [4] A. Ahmad, M. S. Alam, and R. Chabaan, “A comprehensive review of wireless charging technologies for electric vehicles,” *IEEE Trans. Transport. Electric.*, vol. 4, no. 1, pp. 38–63, Mar. 2018.
- [5] Z. Cong, M. Hongbo, L. Jih-Sheng, and Z. Lanhua, “Design considerations to reduce gap variation and misalignment effects for the inductive power transfer system,” *IEEE Trans. Power Electron.*, vol. 30, no. 11, pp. 6108–6119, Nov. 2015.

- [6] M. Budhia, G. Covic, and J. Boys, "Design and optimization of circular magnetic structures for lumped inductive power transfer systems," *IEEE Trans. Power Electron.*, vol. 26, no. 11, pp. 3096–3108, Nov. 2011.
- [7] R. Bosshard, J. W. Kolar, J. Muhlethaler, I. Stevanovic, B. Wunsch, and F. Canales, "Modeling and η - α -Pareto optimization of inductive power transfer coils for electric vehicles," *IEEE J. Emerg. Sel. Topics Power Electron.*, vol. 3, no. 1, pp. 50–64, Mar. 2015.
- [8] M. Budhia, G. Covic, and J. Boys, "A new IPT magnetic coupler for electric vehicle charging systems," in *Proc. 36th Annu. Conf. IEEE Ind. Electron. Soc.*, Glendale, AZ, USA, Nov. 2010, pp. 2487–2492.
- [9] Y. Nagatsuka, N. Ehara, Y. Kaneko, S. Abe, and T. Yasuda, "Compact contactless power transfer system for electric vehicles," in *Proc. IPEC*, Singapore, Jun. 2010, pp. 807–813.
- [10] M. Budhia, J. T. Boys, G. A. Covic, and C.-Y. Huang, "Development of a single-sided flux magnetic coupler for electric vehicle IPT charging systems," *IEEE Trans. Ind. Electron.*, vol. 60, no. 1, pp. 318–328, Jan. 2013.
- [11] A. Zaheer, G. A. Covic, and D. Kacprzak, "A bipolar pad in a 10-kHz 300-W distributed IPT system for AGV applications," *IEEE Trans. Ind. Electron.*, vol. 61, no. 7, pp. 3288–3301, Jul. 2014.
- [12] A. Zaheer, H. Hao, G. A. Covic, and D. Kacprzak, "Investigation of multiple decoupled coil primary pad topologies in lumped IPT systems for interoperable electric vehicle charging," *IEEE Trans. Power Electron.*, vol. 30, no. 4, pp. 1937–1955, Apr. 2015.
- [13] G. A. Covic, J. T. Boys, M. L. G. Kissin, and H. G. Lu, "A three-phase inductive power transfer system for roadway-powered vehicles," *IEEE Trans. Ind. Electron.*, vol. 54, no. 6, pp. 3370–3378, Dec. 2007.
- [14] M. Budhia, G. A. Covic, and J. T. Boys, "Magnetic design of a three-phase inductive power transfer system for roadway powered electric vehicles," in *Proc. IEEE Vehicle Power Propuls. Conf.*, Sep. 2010, pp. 1–6.
- [15] A. Safaee, K. Woronowicz, and T. Dickson, "Reactive power compensation in three phase high output inductive power transfer," in *Proc. EPEC*, Oct. 2015 pp. 375–380.
- [16] A. Safaee, K. Woronowicz, and A. Maknouninejad, "Reactive power compensation scheme for an imbalanced three-phase series-compensated wireless power transfer system with a star-connected load," in *Proc. IEEE Transp. Electrification Conf. Expo (ITEC)*, Jun. 2018, pp. 44–48.
- [17] H. Matsumoto, Y. Neba, K. Ishizaka, and R. Itoh, "Model for a three-phase contactless power transfer system," *IEEE Trans. Power Electron.*, vol. 26, no. 9, pp. 2676–2687, Sep. 2011.
- [18] H. Matsumoto, Y. Neba, H. Iura, D. Tsutsumi, K. Ishizaka, and R. Itoh, "Trifoliate three-phase contactless power transformer in case of winding-alignment," *IEEE Trans. Ind. Electron.*, vol. 61, no. 1, pp. 53–62, Jan. 2014.
- [19] S. Kim, G. A. Covic, and J. T. Boys, "Tripolar pad for inductive power transfer systems for EV charging," *IEEE Trans. Power Electron.*, vol. 32, no. 7, pp. 5045–5057, Jul. 2017.
- [20] S. Kim, G. Covic, and J. T. Boys, "Comparison of tripolar and circular pads for IPT charging systems," *IEEE Trans. Power Electron.*, vol. 33, no. 7, pp. 6093–6103, Jul. 2018.
- [21] *Wireless Power Transfer for Light-Duty Plug-In/Electric Vehicles and Alignment Methodology*, Standard SAE J2954, 2016.
- [22] J. Pyrhonen, T. Jokinen, and V. Hrabovcova, *Design of Rotating Electrical Machines*. Hoboken, NJ, USA: Wiley, 2008.
- [23] J. Gieras, *Linear Induction Drives*. Oxford, U.K.: Clarendon Press, 1994.
- [24] F. Y. Lin, G. A. Covic, and J. T. Boys, "Leakage flux control of mismatched IPT systems," *IEEE Trans. Transp. Electrification.*, vol. 3, no. 2, pp. 474–487, Jun. 2017.
- [25] F. Y. Lin, S. Kim, G. A. Covic, and J. T. Boys, "Effective coupling factors for series and parallel tuned secondaries in IPT systems using bipolar primary pads," *IEEE Trans. Transp. Electrification.*, vol. 3, no. 2, pp. 434–444, Jun. 2017.
- [26] C. Shuwei, L. Chenglin, and W. Lifang, "Research on positioning technique of wireless power transfer system for electric vehicles," in *Proc. IEEE Conf. Expo Transp. Electrification Asia-Pacific (ITEC Asia-Pacific)*, Aug./Sep. 2014, pp. 1–4.
- [27] J. P.-W. Chow, H. S.-H. Chung, and C.-S. Cheng, "Use of transmitter-side electrical information to estimate mutual inductance and regulate receiver-side power in wireless inductive link," *IEEE Trans. Power Electron.*, vol. 31, no. 9, pp. 6079–6091, Sep. 2016.
- [28] M. Ranjram, G. Simeonov, and P. W. Lehn, "A high step-up transformerless DC/DC converter with flat efficiency," in *Proc. 40th Annu. Conf. IEEE Ind. Electron. Soc.*, Dallas, TX, USA, Oct./Nov. 2014, pp. 1034–1040.
- [29] Y. Chen, B. Yang, Z. Kou, Z. He, G. Cao, and R. Mai, "Hybrid and reconfigurable IPT systems with high-misalignment tolerance for constant-current and constant-voltage battery charging," *IEEE Trans. Power Electron.*, vol. 33, no. 10, pp. 8259–8269, Oct. 2018.
- [30] Q.-T. Duong and M. Okada, "Maximum efficiency formulation for multiple-input multiple-output inductive power transfer systems," *IEEE Trans. Microw. Theory Techn.*, vol. 66, no. 7, pp. 3463–3477, Jul. 2018.



Mehanathan Pathmanathan (S'10–M'16) received the B.E. (Hons.) and Ph.D. degrees in electrical and electronic engineering from The University of Adelaide, Adelaide, Australia, in 2007 and 2012, respectively.

From 2012 to 2018, he was a Research Engineer with the Machines and Drives Team, ABB Corporate Research, Västerås, Sweden. Since 2018, he has been a Research Associate with the University of Toronto, Toronto, ON, Canada. His current research interests include synchronous machine excitation systems, medium voltage drive topologies, and wireless power transfer.



Shuang Nie (S'18) received the B.A.Sc. degree (Hons.) in electrical and computer engineering from the University of Toronto, Toronto, ON, Canada, in 2017, where he is currently pursuing the M.A.Sc. degree.

His current research interests include the design of inductive power transfer (IPT) systems for charging electric vehicles.



Netan Yakop received the B.A.Sc. degree in electrical engineering from the University of Toronto, Toronto, ON, Canada, in 2018, where he is currently pursuing the M.A.Sc. degree.

His current research interests include the application of power electronics in electric vehicles and power systems.



Peter W. Lehn (SM'05) received the B.Sc. and M.Sc. degrees in electrical engineering from the University of Manitoba, Winnipeg, MN, Canada, in 1990 and 1992, respectively, and the Ph.D. degree from the University of Toronto, Toronto, ON, Canada, in 1999.

In 1999, he joined the University of Toronto, as a Faculty. He spent six months as a Visiting Professor with the University of Erlangen–Nuremberg, Erlangen, Germany, in 2001. His current research interests include HVdc technologies, grid integration

of storage and renewables, power electronics for electric vehicles, and theoretical analysis of power electronic systems.

Dr. Lehn has been an Editor of the IEEE TRANSACTIONS ON ENERGY CONVERSION from 2013 to 2019.